Available online at www.sciencedirect.com
SCIENCE DIRECT
Journal of Solid State Chemistry 179 (2006) 1076–1085
JOURNAL OF SOLID STATE CHEMISTRY
www.elsevier.com/locate/jssc

A-site cation ordering in $AA'BB'O_6$ perovskites

Meghan C. Knapp, Patrick M. Woodward*

The Ohio State University, Department of Chemistry, 100 West 18th Avenue, Columbus, OH 43210-1185, USA

Received 6 August 2005; received in revised form 30 December 2005; accepted 2 January 2006
Available online 3 February 2006

Abstract

Unlike ordering of the octahedral B-site cations, ordering of the larger A-site cations in stoichiometric perovskites is rare. Herein the A- and B-site ordering characteristics of several double perovskites with $AA'BB'O_6$ stoichiometry have been investigated. The compounds investigated include $NaLaMgWO_6$, $NaLaMgTeO_6$, $NaLaScNbO_6$, $NaLaScSbO_6$, $NaLaTi_2O_6$, and $NaLaZr_2O_6$. Group theoretical methods are used to enumerate the possible structures of $AA'BB'X_6$ double perovskites that result from the combination of rock salt ordering of the B-site cations, layered ordering of the A-site cations, and octahedral tilting distortions. This combination results in 12 possible structures in addition to the aristotype. Among the compounds investigated only $NaLaMgWO_6$ and $NaLaScNbO_6$ show significant long-range ordering of the A-site cations, Na^+ and La^{3+}. A complete structural characterization is presented for $NaLaMgWO_6$. This compound possesses monoclinic $C2/m$ (#12) space group symmetry, with unit cell dimensions of $a = 7.8074(1)$ Å, $b = 7.8158(1)$ Å, $c = 7.8977(1)$ Å, $\beta = 90.136(1)^\circ$ at room temperature. The results presented here show that in $AA'BB'O_6$ perovskites layered ordering of A-site cations creates a bonding instability that is compensated for by a second-order Jahn–Teller distortion of the B' cation. These two distortions are synergistic and the removal of one leads to the disappearance of the other.

Keywords: Perovskites; Cation ordering; X-ray powder diffraction; second-order Jahn–Teller distortions; Complex oxides

1. Introduction

The perovskite structure, stoichiometry ABX_3, is one of the most common oxide structures known, and has been studied extensively. The undistorted structure is cubic, space group $Pm\bar{3}m$, and consists of a three-dimensional network of corner-sharing BX_6 octahedra with A-site cations located centrally in a cube of 8 BX_6 octahedra. The structure can be altered by substituting multiple cations at either the A- or the B-sites. Ordering of the octahedral site cations in $A_2BB'X_6$ perovskites is well known, and the alterations of the symmetry of both the undistorted aristotype (space group $Fm\bar{3}m$), and the distorted hettotypes have been analyzed via group theoretical methods [1–3]. In contrast, ordering of the A-site cations is typically seen only in anion deficient perovskites [4], such as the superconducting $YBa_2Cu_3O_{7-x}$ [5,6], double-perovskites such as $LnBaFe_2O_{5+x}$ [7–9], or triple perovskites such as $YBa_2Fe_3O_{8+x}$ [10]. The preparation and characterization of different polymorphs of $BaLaMn_2O_6$ provide a particularly illustrative example of the close link between layered ordering of the A-site cations and oxygen vacancies [11,12]. When prepared directly the Ba^{2+} and La^{3+} ions in $BaLaMn_2O_6$ are disordered. However, under proper conditions the oxygen deficient perovskite, $BaLaMn_2O_5$, can be prepared where the Ba^{2+} and La^{3+} ions order in layers and the oxygen vacancies are exclusively found in the lanthanum layer. If $BaLaMn_2O_5$ is oxidized at low temperature the oxygen vacancies can be filled without destroying the A-site cation ordering, to form the metastable $BaLaMn_2O_6$ where the layered Ba^{2+}/La^{3+} ordering is retained.

Several recent studies of nonstoichiometric perovskites, $A_{1-x}MO_3$, report layered ordering of the A-site cation vacancies [13–15]. Various degrees of layered ordering have also been observed in $A_{1-x}A'_yMO_3$ compounds with a mixture of two different cations and vacancies on the A-sites. For example, the compound $(Li_{3x}La_{2/3-x})TiO_3$,

*Corresponding author. Fax: +614 292 0368.
E-mail addresses: mknapp@chemistry.ohio-state.edu, woodward@chemistry.ohio-state.edu (P.M. Woodward).

0022-4596/$ - see front matter © 2006 Elsevier Inc. All rights reserved.
doi:10.1016/j.jssc.2006.01.005

studied extensively for its lithium ion conductivity, shows A-site cation ordering for small values of x, where the A-site cation vacancy concentration is relatively high ($x>0.08$), but A-site cation ordering is absent in the stoichiometric end member, $LiLaTi_2O_6$ [16–18]. Careful examination of the structure and microstructure of $(Li_{3x}La_{2/3-x})TiO_3$ through X-ray diffraction and electron microscopy has shown that in addition to composition, the thermal history of these compounds plays a role in the degree of ordering [19]. The distortions of these structures have also been analyzed by group theoretical methods [20,21]. Another example of partial ordering of cations and vacancies on the A-site cation positions was recently reported for $La_4Mg_3W_3O_{18}$ where layers fully occupied by La^{3+} are observed to alternate with layers where 2/3 of the A-site cation positions are vacant [25].

Examples of A-site cation ordering in stoichiometric $AA'M_2X_6$ and $AA'BB'X_6$ perovskites, where there are neither anion vacancies nor A-site cation vacancies, are exceedingly rare [23]. The metastable form of $BaLaMn_2O_6$ has already been mentioned. Another example is the partial ordering of Nd^{3+} and Ag^{+}, observed in $NdAgTi_2O_6$ samples prepared under high-pressure conditions [22]. In 1984 Sekiya et al. published the structure of $NaLaMgWO_6$ [24]. This compound is reported to exhibit both rock salt ordering of the B-site cations and layered ordering of the A-site cations. Interestingly, the seemingly analogous perovskite $NaLaTi_2O_6$ does not seem to show long-range A-site cation ordering. These observations suggest that A-site cation ordering may be more prevalent in the presence of B-site cation ordering, but the relationship between the two is not at all understood. Furthermore, the crystallographic details that result from the combination of (a) layered ordering of the A-site cations, (b) rock salt ordering of the B-site cations and (c) octahedral tilting distortions have not been previously investigated. These points are the focus of this paper.

2. Experimental details

$NaLaMgWO_6$ was prepared from the solid state reaction between $MgWO_4$, Na_2CO_3 (Fisher) and La_2O_3 (GFS) by heating first to 900 °C for 6 h and then to 1050 °C for 18 h in a Carbolite furnace. A 10% excess of Na_2CO_3 was used to account for high-temperature volatility, and a 17% excess of La_2O_3 was used to account for the absorption of water. This latter amount was calibrated from thermogravimetric measurements of $La_2O_3 \cdot nH_2O$. $MgWO_4$ was prepared from MgO (Allied) and WO_3 (Cerac) by ceramic methods, using an excess of 15% MgO. Once $NaLaMgWO_6$ was prepared it was stored in a desiccator because previous preparations were prone to decomposition in ambient air over time. $NaLaScSbO_6$, $NaLaScNbO_6$, $NaLaMgTeO_6$, $NaLaTi_2O_6$ and $NaLaZr_2O_6$ were also synthesized by ceramic methods, in each case directly from Na_2CO_3 and the appropriate binary metal oxides. Starting materials for these materials included TeO_2 (Cerac), Sc_2O_3 (Boulder), Nb_2O_5 (Aldrich), Sb_2O_3 (Cerac), TiO_2 (GFS), and ZrO_2 (Johnson Matthey). Final annealing temperatures were 1100 °C for $NaLaMgTeO_6$, $NaLaScNbO_6$ and $NaLaZr_2O_6$; 1000 °C for $NaLaScSbO_6$; and 1050 °C for $NaLaTi_2O_6$.

X-ray powder diffraction data were collected in Bragg-Brentano geometry using a Bruker D8 X-ray powder diffractometer (40 kV, 50 mA, sealed Cu X-ray tube) equipped with an incident beam Ge 1 1 1 monochromator and a Braun linear position sensitive detector. Structure refinements were performed using the Rietveld method [26] as implemented in the TOPAS software package [27]. Group theoretical analysis of these systems was aided by the program ISOTROPY developed by Harold Stokes and Dorian Hatch at Brigham Young University (stokes.byu.edu/isotropy.html) [28].

3. Results

3.1. Layered ordering vs. rock salt ordering

It is worthwhile to first examine the tendency for A-site cation ordering, when present, to occur in a layered fashion, rather than in the rock salt pattern commonly observed for B-site cations. From an electrostatic point of view rock salt ordering must also be preferable for A-site cations, yet long-range rock salt ordering of A-site cations is very rare. To the best of our knowledge there is only one example of long-range rock salt ordering of A-site cations, $Na_2BaFe_4F_{12}$, which exhibits an ordered distribution of sodium cations on one crystallographic site and barium cations and vacancies on another site. Interestingly in this compound the Na–F and Ba–F bond distances are equivalent, as required by the space group symmetry [29]. The near complete absence of rock-salt ordering of A-site cations in perovskites can be traced to the anion environment. Ordering of the cations is generally favored when there is a significant difference in size and/or charge of the cations [4]. These differences serve as the driving force for the cations to occupy crystallographically distinct positions within the structure. In the absence of a significant charge and/or size mismatch a disordered cation arrangement will typically be favored. The perovskite anion is coordinated by two B-site cations and four A-site cations. The B-site cations are on opposite sides from one another, as shown in Fig. 1a. Thus, when there is a rock salt ordering of B and B' ions with different radii the anion may easily shift towards the smaller cation and away from the larger cation to relieve lattice strains arising from the size mismatch. This is reflected in the subgroup that results from this distortion, $Fm\bar{3}m$, where the anion sits on the Wyckoff position 24e (x, 0, 0).

If A and A' are ordered in a rock salt fashion the resulting space group symmetry is once again $Fm\bar{3}m$, but the anion now resides on a position with no variable parameters, Wyckoff site 24d ($0, \frac{1}{4}, \frac{1}{4}$). In this structure there is no mechanism for the anion to displace in response to a

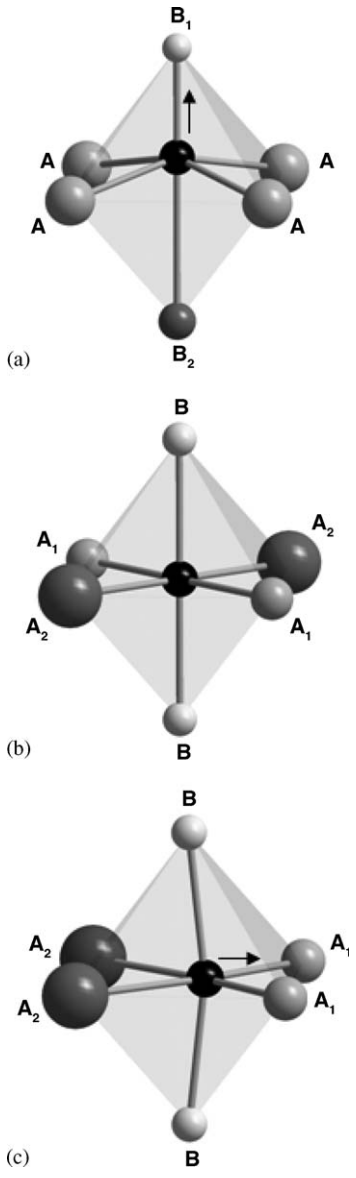

Fig. 1. The anion environment for perovskites exhibiting: (a) rock salt ordering of the *B*-site cations; (b) rock salt ordering of the *A*-site cations; and (c) layered ordering of the *A*-site cations.

size mismatch between A and A', as can be seen in Fig. 1b. Thus, rock salt ordering of A-site cations will be unfavorable when there is a significant mismatch in the radii of the A and A' cations. Alternatively the A-cations can order in layers. Layered ordering of an $AA'B_2X_6$ perovskite results in $P4/mmm$ space group symmetry. This arrangement leads to three chemically distinct environments for the anions. Two-thirds of the anions sit on the $4i$ Wyckoff position. These ions are surrounded by two B-site cations, two A-site cations and two A'-site cations, as shown in Fig. 1c. This environment enables the anion to shift toward the layer with the smaller and/or more highly charged A-site cation. While this type of ordering helps to accommodate the size mismatch, the electrostatic interactions associated with this arrangement are less favorable. Another undesirable feature is that 1/6 of the anions sit on the $1b$ Wyckoff position and are surrounded by 4 A-site cations and 2 B-site cations, while another 1/6 of the anions sit on the $1a$ Wyckoff position and are surrounded by 4 A'-site cations and 2 B-site cations. This creates a structural instability when the sizes and/or bonding strengths of the A and A' cations are significantly different. Thus layered ordering of A-site cations only partially alleviates the lattice strains associated with an A/A' size mismatch. We will return to this point later.

3.2. *A-site cation ordering (layered), B-site cation ordering (rock salt) and octahedral tilting*

Analysis of the symmetry reduction from the aristotype perovskite structure in response to ordering of the cations and tilting of the octahedra was completed using the online version of ISOTROPY. Starting with the parent perovskite structure with $Pm\bar{3}m$ (221) space group symmetry, the distortions for ordering were entered. Ordering of the B-site cations in a rock salt fashion is a basis for the one-dimensional R_1^+ irreducible representation (irrep), following the notation of Miller and Love [30]. Ordering of the A-cations in layers is a basis for the three-dimensional X_3^- irrep. The three parameters of this irrep may be listed as (a, b, c). When two of the parameters are equal, they are given the same letter. If the parameters are all 0, there is no distortion. Layered ordering of the A-cations occurs when the parameters are (a, 0, 0). The structure which allows both rock salt ordering of the B-site cations and layered ordering of the A-site cations has $P4/nmm$ space group symmetry, and is an isotropy subgroup of $Pm\bar{3}m$. However, if the symmetry is lowered slightly, the parameter sets (a, b, 0), (a, a, b), and (a, b, c) allow, but do not require layered ordering. That is, the resulting crystal structures will have more than one crystallographic site for the A-site cations in each layer. This arrangement allows for A-site ordering, but does not require a fully ordered arrangement. While these possibilities do not affect the selection of $P4/nmm$ as the aristotype space group, their inclusion is necessary to carry out a complete analysis of subgroups caused by octahedral tilting.

The program ISOTROPY may further be used to determine the symmetry changes upon rotations of polyhedra, in this case of the BX_6 octahedra. Such distortions may be in-phase, where the rotations along a particular axis are in the same direction from one layer to the next, or out-of-phase, in which case the rotations are in opposite directions. These rotations may be analyzed either beginning with the $P4/nmm$ cation ordered structure, or from the parent space group $Pm\bar{3}m$. The analysis shown here considers the cation ordering and the octahedral rotations in combination at the same time, and thus what follows is an analysis from the parent perovskite space group. Analysis beginning from the ordered $P4/nmm$ aristotype yields the same results. In-phase tilting distortions are bases for the three-dimensional irrep M_3^+ in

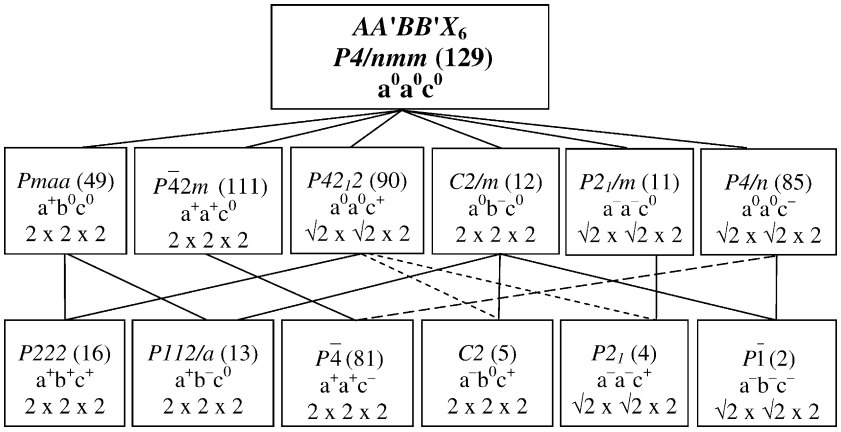

Fig. 2. A schematic diagram showing possible structures generated by octahedral tilting distortions in perovskites exhibiting layered ordering of the *A*-site cations, and rock salt ordering of the *B*-site cations. Each box shows the space group, tilt system using Glazer's notation [50], and approximate cell dimensions in terms of the cell edge of the undistorted $Pm\bar{3}m$ perovskite. The lines indicate group–subgroup relationships, where the solid lines represent possible continuous transitions and the dashed lines represent discontinuous transitions.

$Pm\bar{3}m$, while out-of-phase tilting distortions are bases for the three-dimensional irrep R_4^+. Only simple tilts were considered, as defined by Howard and Stokes [31], in which tilting along a particular axis, if it exists, is either in-phase, or out-of-phase, but not both simultaneously. The results of this symmetry analysis are shown in Fig. 2.

There are 12 different combinations of octahedral tilting, rock salt ordering of the *B*-site cations and layered ordering of the *A*-site cations that result. As expected, tilt systems that involve only rotations about the *c*-axis, $a^0a^0c^-$ and $a^0a^0c^+$, retain the tetragonal symmetry of the $P4/nmm$ aristotype. In-phase tilts of equal magnitude about the *a*- and *b*-axes, $a^+a^+c^0$, also retain the tetragonal symmetry, although this distortion requires an expansion of the unit cell in the *ab* plane. Interestingly, the structure retains the unit cell of the aristotype structure upon undergoing out-of-phase tilts of equal magnitude about the *a*- and *b*-axes, $a^-a^-c^0$, but the symmetry is lowered to monoclinic. Further combinations of these basic types of tilting lower the symmetry further. The absence of tilt systems such as $a^-a^-c^-$ (or $a^+a^+c^+$) is due to the fact that adding a tilt about the *c*-axis destroys sufficient symmetry elements so that the tilts about the *a*- and *b*-axes are no longer required to be of equal magnitude. Therefore, by symmetry $a^-a^-c^-$ (or $a^+a^+c^+$) is not distinct from $a^-b^-c^-$ (or $a^+b^+c^+$). This criterion for identifying unique tilt systems has been used previously by Howard and Stokes [31].

4. Structural characterization

4.1. $NaLaMgWO_6$

The X-ray powder pattern of $NaLaMgWO_6$ is shown in Fig. 3. The strong peaks with indices (111) and (311) clearly indicate the presence of rock salt ordering of *B*-site cations. Similarly, the (001) and (201) peaks are evidence of layered *A*-site cation ordering. While the pattern can be refined in the parent space group, $P4/nmm$, the peak profiles,

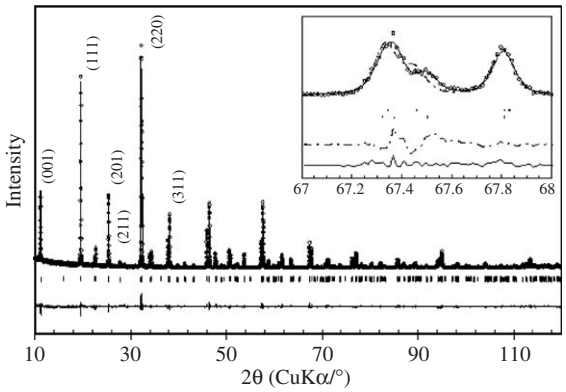

Fig. 3. The observed X-ray powder diffraction pattern (open circles) along with calculated and difference patterns from the Rietveld refinement of $NaLaMgWO_6$. The vertical tick marks indicate the expected 2θ positions of the reflections. The inset compares the Rietveld refinement of the pattern in space group $C2/m$ (solid line, $R_{wp} = 0.145$) and $P2_1/m$ (dashed line $R_{wp} = 0.155$) for the pseudo-cubic $\langle 440 \rangle$ and $\langle 225 \rangle$ set of peaks. The upper set of tick marks and difference pattern refer to the $P2_1/m$ refinement, the lower to $C2/m$.

particularly of the pseudo-cubic $\langle 440 \rangle$ reflections, clearly indicate lower symmetry. If the reduction in symmetry is the result of octahedral tilting, the structure should belong to a space group that is contained in Fig. 2. Our initial attempts to analyze the X-ray powder data were carried out with a $P2_1/m$ starting model, as this was the space group assignment by Sekiya et al. [24] and subsequently Arillo et al. [32]. While the assignment to the space group $P2_1/m$ is consistent with the distortion $a^-a^-c^0$ in Fig. 2, this assignment is not consistent with the observed reflection splitting. To find the correct crystal structure we analyzed the reflection splitting and systematic absences and compared the observations with the possible structures obtained from the group theoretical analysis presented above (see Fig. 2). Based on this analysis we conclude that $NaLaMgWO_6$ possesses $C2/m$ space group symmetry. The crystal structure is described in Table 1. It belongs to the

Table 1
Crystallographic data for $NaLaMgWO_6$, space group $C2/m$

Atom	Wyckoff site	x	y	z	B_{iso} (Å^2)[a]
Na	4*g*	0	0.243(3)	$\frac{1}{2}$	0.66(6)
La	4*h*	0	0.2494(5)	0	0.66(6)
Mg	4*i*	0.748(2)	0	0.745(1)	0.21(5)
W	4*i*	0.2489(3)	0	0.7331(1)	0.21(5)
O(1)	4*i*	0.005(4)	0	0.706(4)	2.4(3)
O(2)	8*j*	0.750(3)	0.259(3)	0.767(3)	2.4(3)
O(3)	4*i*	0.701(3)	0	0.492(2)	2.6(3)
O(4)	4*i*	0.496(4)	0	0.790(5)	2.4(3)
O(5)	4*i*	0.786(4)	0	0.998(2)	3.3(6)

$a = 7.8074(1)$ Å, $b = 7.8158(1)$ Å, $c = 7.8977(1)$ Å, $\beta = 90.136(1)^\circ$ and $R_{wp} = 0.1449$. Estimated standard deviations are given in parentheses.

[a]Constraints were placed on the atomic displacement factors for the *A*-site cations Na = La; the *B*-site cations Mg = W; and the equatorial oxygen sites O(1) = O(2) = O(4).

tilt system $a^0b^-c^0$, where the b^- indicates an out-of-phase tilt about the *b*-axis.

The difference between the previously proposed $a^-a^-c^0$ structure, which has a $\sqrt{2}a_p \times \sqrt{2}a_p \times 2a_p$ unit cell with $P2_1/m$ symmetry, and our proposed $a^0b^-c^0$ structure, which has a $2a_p \times 2a_p \times 2a_p$ unit cell with $C2/m$ space group symmetry, (a_p is the cell edge of the simple cubic perovskite structure) is fairly subtle. The absences created by the C-centering of the $a^0b^-c^0$ structure compensate for the smaller unit cell of the $a^-a^-c^0$ structure. As such, the two structures give rise to superstructure reflections at essentially the same Bragg angles, and it is necessary to rely on differences in peak splitting to differentiate between the two. Even the differences in peak splitting are subtle, so that the effects are most clearly seen at high angles. The inset to Fig. 3 shows the fit to the pseudo-cubic ⟨440⟩ reflections obtained using the $C2/m$ structure (solid line), as well as the fit obtained using the $P2_1/m$ structure (dashed line). The observed peak splitting clearly cannot be accounted for using the $P2_1/m$ model, essentially ruling out tetragonal and orthorhombic space groups with $\sqrt{2}a_p \times \sqrt{2}a_p \times 2a_p$ unit cells. In contrast, a good fit can be obtained with the $2a_p \times 2a_p \times 2a_p$ cell of the $a^0b^-c^0$ structure.

Refinements were completed using structural models belonging to the space groups $C2/m$ ($a^0b^-c^0$), $C2$ ($a^-b^0c^+$), and $P2/c$ ($a^-b^+c^0$). The fit obtained with $a^-b^+c^0$ was inferior to those obtained in the other two tilt systems and was not considered further. The refined fit to the data was not improved by lowering the symmetry from $C2/m$ to $C2$. Hence, the higher symmetry $C2/m$ space group symmetry was preferred. The Rietveld refinement yielded a goodness-of-fit parameter, R_{wp}, equal to 0.145. This compares favorably to the goodness-of-fit parameter obtained from whole pattern fitting using the Pawley method, $R_{wp} = 0.140$. The similarity between these two values strongly supports the validity of the refined structure. The observed, calculated and difference patterns are shown in Fig. 3.

To investigate the possibility of partial disordering of cations, the Na and La ions, as well as the W and Mg ions, were allowed to mix during the refinements. This did little to improve the quality of the fits and both the *A*- and *B*-site occupancies refined to values that varied little from the fully ordered structure. Therefore, the ordering on both the *A*- and *B*-sites was taken to be complete. The thermal displacement parameters of the *A*-site cations were constrained to be equal, as were those of the *B*-site cations. Axial oxygen, O(3) and O(5), displacement parameters were refined individually, while the displacement parameters of the equatorial oxygen ions, O(1), O(2) and O(4), were constrained to be equal. This was done to prevent unwanted correlations between individual displacement parameters.

4.2. Additional $NaLaBB'O_6$ and $NaLaB_2O_6$ perovskites

To further investigate the relationship between cation ordering on the *A*- and *B*-sites several additional samples were prepared and characterized. X-ray powder data were collected for additional samples using the Bruker D8 X-ray diffractometer. Pawley fits were completed on these structures in the space groups $P4/nmm$ ($NaLaScNbO_6$ and $NaLaMgTeO_6$), $Fm\bar{3}m$ ($NaLaScSbO_6$), and $Pnma$ ($NaLaTi_2O_6$ and $NaLaZr_2O_6$). For this manuscript the discussion is limited to the cation ordering characteristics of these compounds. The basic features of these structures, as extracted from Rietveld refinements, are summarized in Table 2. A full analysis of the structural features of these compounds using neutron powder diffraction data is in progress and will be published at a later date.

The X-ray powder diffraction patterns of the six compounds investigated in this study are compared in Fig. 4. Shaded regions denote the positions where the strongest cation ordering reflections are expected. The peak at ~19–20° 2θ, which corresponds to the 1 1 1 reflection on a $2a_p \times 2a_p \times 2a_p$ cell, is characteristic of rock salt ordering, as is the 3 1 1 reflection. The peak at ~11° 2θ, which corresponds to the 0 0 1 reflection on a $2a_p \times 2a_p \times 2a_p$ cell, is the signature of layered cation ordering. The 2 0 1 and 2 2 1 peaks are also indicative of this type of ordering. As previously discussed, $NaLaMgWO_6$ exhibits both Mg/W rock salt ordering and Na/La layered ordering. $NaLaScNbO_6$ is the only other compound that was investigated in this study which exhibits dual ordering of both the *A*- and *B*-site cations, although Rietveld refinements indicate that the Na/La and Sc/Nb distributions are only 62% and 84% ordered, respectively. The degree of cation ordering is quantified with the long-range order parameters:

$$\mathrm{LRO}(A) = 2 \times S_A^A - 1,$$

$$\mathrm{LRO}(B) = 2 \times S_B^B - 1,$$

where S_A^A is the fractional occupancy of the *A* cation on the site that is predominantly occupied by *A* cation, as opposed to the *A'* cation. For example in $LaNaScNbO_6$ the site

Table 2
Structural characteristics and cation ordering in a variety of $NaLaBB'O_6$ compositions

Compound	Tol. factor	Space group	Tilt system	*A*-site order[a] (%)	*B*-site order[a] (%)
$NaLaMgWO_6$	0.94	$C2/m$	$a^0b^-c^0$	100	100
$NaLaMgTeO_6$	0.95	$P4/nmm$	$a^0a^0c^0$	<10	100
$NaLaScNbO_6$	0.95	$P4/nmm$	$a^0a^0c^0$	62	84
$NaLaScSbO_6$[b]	0.94	$Fm3m$	$a^0a^0a^0$	Trace[b]	100
$NaLaZr_2O_6$[b]	0.93	$Pnma$	$a^-b^+a^-$	Trace[b]	—
$NaLaTi_2O_6$	0.98	$Pnma$	$a^-b^+a^-$	0	—

[a]Cation order is calculated from the site occupancies as defined in the text.
[b]Evidence of *A*-site cation ordering in these compounds is inferred from the appearance of a weak, broad 0 0 1 peak after prolonged annealing, which made it difficult to accurately estimate the degree of order. If present on a long-range scale this ordering would change the space group symmetry to $P4/nmm$ ($NaLaScSbO_6$) and to $P2_1/c$ ($NaLaZr_2O_6$).

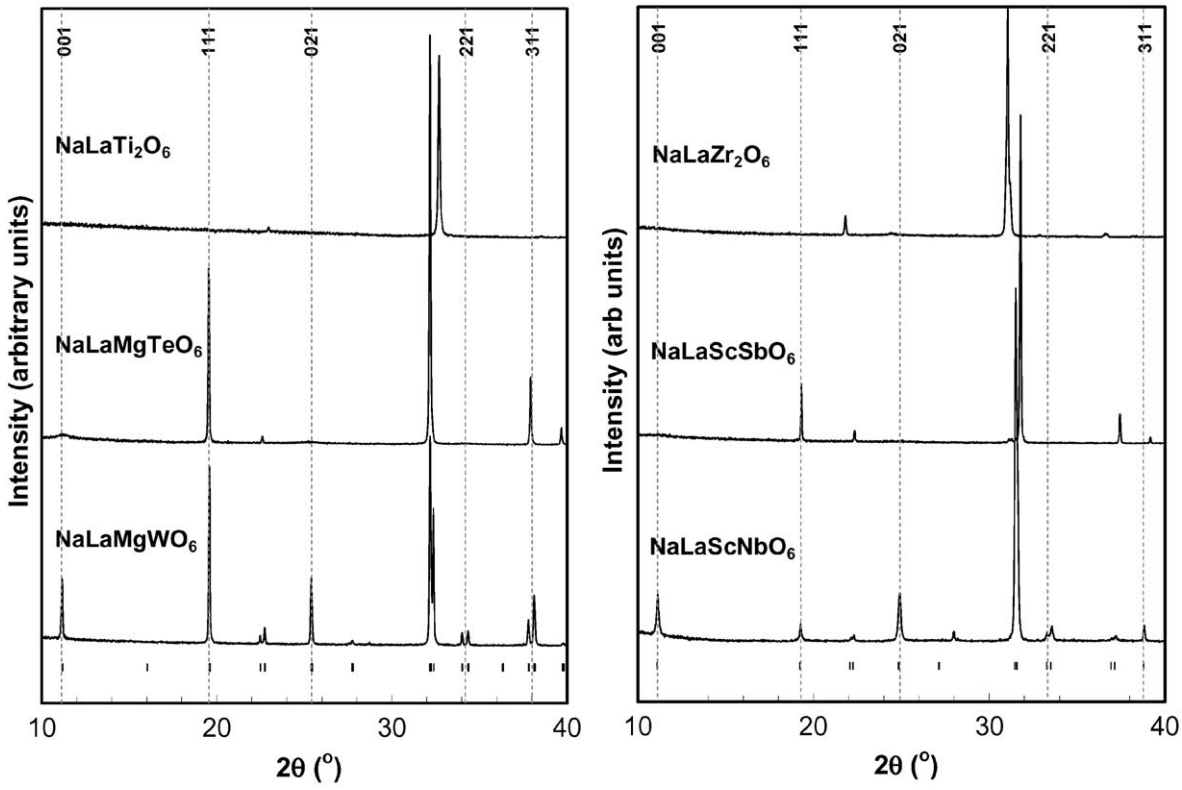

Fig. 4. X-ray powder diffraction patterns are shown for $NaLaMgWO_6$, $NaLaMgTeO_6$, $NaLaTi_2O_6$ on the left, and $NaLaScNbO_6$, $NaLaScSbO_6$, $NaLaZr_2O_6$ on the right. The reflection markers at the bottom denote the expected peak positions for $NaLaMgWO_6$ and $NaLaScNbO_6$, respectively. Shaded areas show the locations of select peaks that originate from cation ordering. The 001, 021 and 221 peaks are indicative of layered cation order, while the 111 and 311 peaks are indicative of rock salt cation order. The peaks are indexed on a doubled pseudo-cubic, $2a_p \times 2a_p \times 2a_p$, unit cell.

preferentially occupied by lanthanum contains 81% La^{3+} and 19% Na^+, and the inverse occupancies apply to the sodium site. The *B*-site LRO parameter is calculated in an analogous manner. The *B*-site cation distribution is fully ordered in $NaLaMgTeO_6$ and $NaLaScSbO_6$, but interestingly there is little sign of long-range order of the *A*-site cations in these two compounds. There is a weak and broad 0 0 1 reflection in $NaLaMgTeO_6$, which suggests the presence of short to medium range Na/La ordering. The width of the peak indicates that the coherent size of the ordered domains is very small. Using the Scherrer formula the size of the ordered domains is estimated from the 0 0 1 reflection to be 40 Å, while the overall crystallite size as estimated from the subcell reflections is at least 1300 Å. There is little indication of long-range *A*-site cation ordering in the other compositions.

5. Discussion

It was pointed out in the earlier discussion that there are three chemically different environments for the anions in $AA'M_2X_6$ and $AA'MM'X_6$ perovskites, which exhibit

layered ordering of *A*-site cations. Let us consider the implications for bonding in a compound such as NaLaMg WO_6. We begin by calculating idealized bond valences in the Pauling sense [33], assuming equal valences for each type of metal-oxygen bond. The bond graph [34–36] for this compound is shown in Fig. 5. The bond valences are calculated by dividing the metal oxidation state by its coordination number: $s(W–O) = 1$, $s(Mg–O) = 1/3$, $s(La–O) = 1/4$ and $s(Na–O) = 1/12$. These valences are chosen to give the correct bond valence sums for the cations. If Pauling's second rule [33] is obeyed they should also give bond valence sums of 2 for each type of oxygen. The bond valence sum at the O_b ion is given by the following summation:

$$\begin{aligned}\mathrm{BVS}(O_b) &= s(Mg{-}O) + s(W{-}O) + 2\times s(La{-}O) \\ &\quad + 2\times s(Na{-}O) \\ &= 1/3 + 1 + 2(1/4) + 2(1/12) = 2.\end{aligned}$$

This matches the ideal value in agreement with Pauling's second law. However, the bond valence sums at the other two oxygen sites violate Pauling's second law:

$$\begin{aligned}\mathrm{BVS}(O_a) &= s(Mg{-}O) + s(W{-}O) + 4\times s(Na{-}O) \\ &= 1/3 + 1 + 4(1/12) = 1.67,\end{aligned}$$

$$\begin{aligned}\mathrm{BVS}(O_c) &= s(Mg{-}O) + s(W{-}O) + 4\times s(La{-}O) \\ &= 1/3 + 1 + 4(1/4) = 2.33.\end{aligned}$$

Thus the O_a ion, which resides in the NaO layer, is underbonded, while the O_c ion, which resides in the LaO layer, is overbonded. Use of quantitative bond valences will alter this picture somewhat, but the underlying bond strains will remain unless the sizes of all cations are perfectly matched.

To better understand how these bond strains are accommodated in $NaLaMgWO_6$ let us consider the bond distances and bond valences in more detail. The bond distances and bond valence sums for $NaLaMgWO_6$ are shown in Table 3. Bond valence sums were calculated using the equation:

$$s_i = \Sigma \exp[(R_0 - R_{ij})/b],$$

where R_0 is an empirical parameter specific to each ion-pair, b is an empirical parameter taken to be equal to 0.37, and R_{ij} is the bond distance reported in Table 3. The values of R_0 were determined by Brown and Altermatt [37]. All bond distances and bond valence sums are reasonable, though the magnesium ion is somewhat overbonded. In Fig. 6, O(1), O(2) and O(4) are equatorial anions corresponding to the O_b ion in the bond graph of Fig. 5, whereas, O(3) is surrounded by four Na^+ ions and corresponds to O_a in the bond graph, and O(5) is surrounded by four La^{3+} corresponding to O_c in the bond

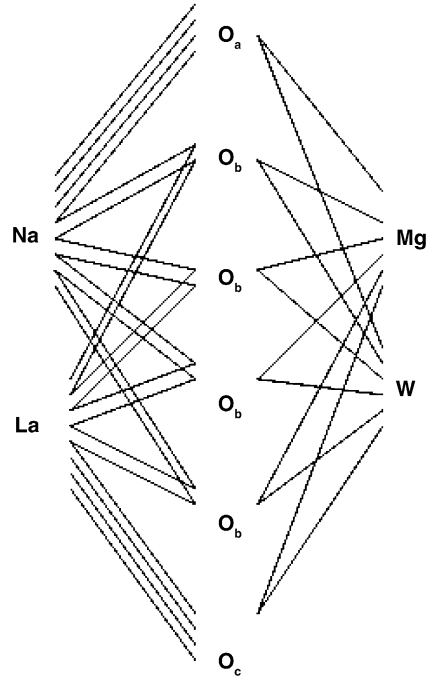

Fig. 5. A bond graph for $NaLaMgWO_6$. The O_a ion resides in the Na layer, corresponding to O(3) in Fig. 6. The O_c ion resides in the La layer, corresponding to O(5) in Fig. 6. The O_b ions reside in the Mg/W layer, corresponding to O(1), O(2) and O(4) in Fig. 6.

Table 3
Bond distances (in Å) for $NaLaMgWO_6$

Atom	Na	La	Mg	W	Oxygen BVS
O(1)	2.50(3) × 2	3.03(2) × 2	2.03(3) × 1	1.92(3) × 1	1.90
O(2)	2.87(2) × 2	2.68(2) × 2	2.03(2) × 2	1.90(2) × 2	2.05
	2.88(2) × 2	2.69(2) × 2			
O(3)	2.55(2) × 2	—	2.03(2) × 1	1.82(2) × 1	2.04
	3.01(2) × 2				
O(4)	3.05(3) × 2	2.57(2) × 2	2.00(3) × 1	1.98(3) × 1	2.04
O(5)	—	2.57(2) × 2	2.02(2) × 1	2.14(2) × 1	1.88
		2.97(2) × 2			
Cation BVS	0.94	2.81	2.45	5.77	

The estimated standard deviations from the Rietveld refinements are given in parentheses. Bond valence sums (BVS) for cations are given at the bottom, and for anions on the right-hand side.

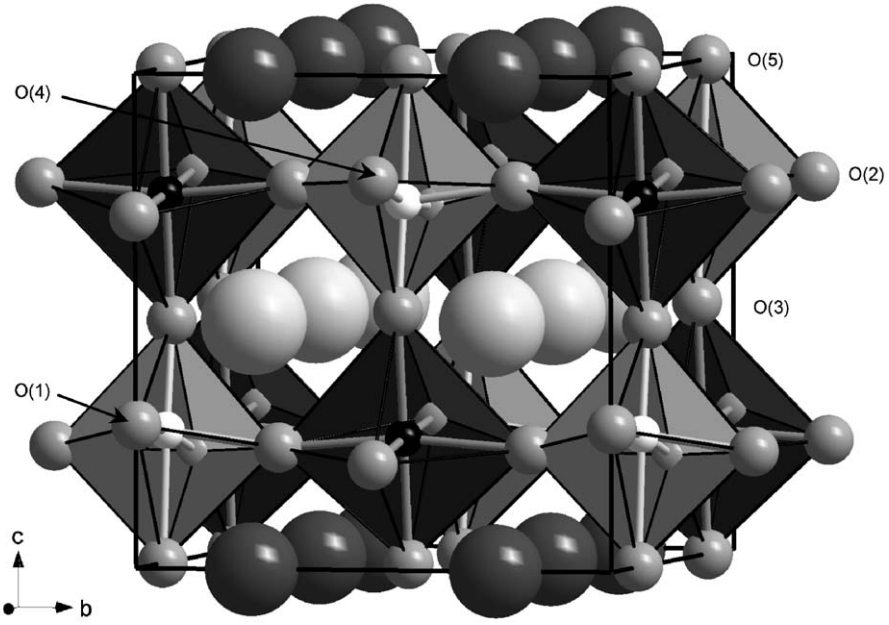

Fig. 6. The crystal structure of $NaLaMgWO_6$. The larger spheres are lanthanum (dark gray) and sodium (light gray). The smaller spheres are magnesium (black), tungsten (white) and oxygen (gray).

graph. Examination of the W–O distances reveals how the structure is able to alleviate the bond strains imposed by the layered ordering of Na^+ and La^{3+} ions. The W^{6+} ion moves away from the overbonded O(5) ion, reducing its valence, and toward the underbonded O(3) ion, increasing its valence. As a result the W–O(3) bond is much shorter, 1.82 Å, than the W–O(5) bond, 2.14 Å. At the same time the Mg-centered octahedron remains fairly symmetric. The structure was analyzed using the program IVTON [51], which revealed that the W^{6+} ion is shifted by 0.19 Å and the Mg^{2+} ion by 0.07 Å from the centers of their respective octhaedra. The tilt angle was estimated from the Mg_c–O–W_c angle, where Mg_c and W_c are the centroids of the magnesium and tungsten octahedra, respectively. No tilting is observered about the *a*- and *c*-axis, so the Mg_c–O(2)–W_c angle, 174.9°, is very close to linear. The Mg_c–O(1)–W_c and Mg_c–O(4)–W_c angles, 160.0° and 165.1°, respectively, are reflective of the tilt about the *b*-axis. Averaging these two angles gives an octahedral rotation of about ~9°, about the *b*-axis.

A significant displacement of the d^0 W^{6+} ion from the center of its octahedral coordination environment is well known in many compounds, including WO_3 [38–40]. The driving force behind this distortion is electronic in nature. It is favored when there is a small energy gap between the empty W 5*d* orbitals and the filled O 2*p* orbitals. This type of distortion is typically referred to as a second-order Jahn–Teller distortion [41,42]. Interestingly such a distortion does not occur in $A_2MW^{6+}O_6$ perovskites (A = Ba, Sr, Ca) that exhibit rock salt order of W^{6+} cations and a larger divalent cation [43–49]. The lack of a second-order Jahn–Teller distortion in rock salt ordered double perovskites comes from the fact that the cooperativity of the W^{6+} displacements, which is necessary to maintain reasonable bond valence sums at oxygen, is disrupted by the M/W ordering. This effect is overcome in $NaLaMgWO_6$ because the Na/La layered ordering and the W^{6+} displacements are synergistic, with each one compensating for the bond strains inherent to the other.

If the above hypothesis is correct, the stability of layered ordering in $AA'BB'X_6$ perovskites should be diminished if the displacements of the B' cation are suppressed. This exact effect can be seen from the collective behavior of the $NaLaBB'O_6$ compounds studied. In $NaLaMgWO_6$ and $NaLaScNbO_6$ the M' cations are d^0 metals in high oxidation states, which are prone to undergo second-order Jahn–Teller distortions. In these compounds a high degree of layered La/Na ordering is observed. On the other hand, when W^{6+} and Nb^{5+} are replaced with isovalent main group cations of similar size, such as Te^{6+} and Sb^{5+}, the electronic driving force for the displacement of the *B*-site cation is removed, which in turn destabilizes layered ordering of the *A*-site cations. This explains the lack of *A*-site cation order in $NaLaMgTeO_6$ and $NaLaScSbO_6$ even though a high degree of *B*-site cation order is maintained in these compounds. The lack of ordering in these two compounds also supports our hypothesis that the second-order Jahn–Teller distortion plays a more important role than simple electrostatics in driving the displacement of the W^{6+} ion toward the NaO^- layer.

It is interesting to consider the behavior of $NaLaZr_2O_6$ and $NaLaTi_2O_6$. As stated before, no indication of long-range cation ordering is observed for the $NaLaTi_2O_6$, and there is little sign of long-range cation ordering in $NaLaZr_2O_6$. Though in $NaLaZr_2O_6$ there are features in the XRD pattern indicative of slight ordering with

prolonged annealing (X-ray pattern not shown). Both of these compounds contain d^0 cations on 100% of the octahedral sites. Apparently this arrangement is less favorable for stabilizing *A*-site cation ordering. While one can imagine various reasons for this behavior, further study is needed to comment definitively.

Finally it is worthwhile to note that the presence of cation displacements does not alter the group theoretical analysis presented earlier. The irrep (X_3^-) that forms a basis for the layered ordering of the *A*-site cations, is the same irrep associated with *B*-site cation displacements. The *B*-site cation can shift in many possible directions. The highest symmetry directions can be described as parallel to the C_4-axis (toward an octahedral corner), the C_3-axis (toward an octahedral face), or the C_2-axis (toward an octahedral edge). These shifts are described by the parameters (a, 0, 0), (a, a, 0) and (a, a, a), respectively. However, only a shift that is primarily along the C_4-axis will help to compensate for the bond strains associated with layered ordering. As such the sets of parameters (a, 0, 0), (a, b, 0), (a, a, b) and (a, b, c) are allowed, in which the shift along one axis may be thought of as being much greater than the other two. Not surprisingly, the irreproducible representations corresponding to these distortions are the same ones associated with layered *A*-site cation ordering. Therefore, the presence of *B*-site cation displacements does not alter the symmetry analysis presented in Fig. 2.

6. Conclusions

The structure of $NaLaMgWO_6$ has been determined from X-ray powder diffraction data. This compound exhibits the unusual combination of layered ordering of the *A*-site cations, rock salt ordering of the *B*-site cations, and $a^0b^-c^0$ octahedral tilting. A group theoretical analysis of the combined effects of these three types of distortions is presented for the first time. While the layered ordering of *A*-site cations, especially in cooperation with anion vacancies, has been previously observed, the connection between displacements of the *B*-site cations and layered ordering of the *A*-site cations has not previously been noted. A second-order Jahn–Teller distortion drives a displacement of the B' cation, which in turn stabilizes layered ordering of the Na^+ and La^{3+} cations. These two distortions are synergistic and the removal of one leads to the disappearance of the other. Of course as with *B*-site cation ordering differences in charge and/or size of the *A* and A' cations will also play a role. $NaLaScNbO_6$ also exhibits both rock salt ordering of Sc^{3+} and Nb^{5+}, and layered ordering of Na^+ and La^{3+}. When the d^0 cations are replaced by main group ions to form $NaLaMgTeO_6$ and $NaLaScSbO_6$, respectively, the second-order Jahn–Teller distortions of the octahedral cations are suppressed and the Na^+/La^{3+} ordering disappears. Based on this work it is anticipated that further examples of dual cation ordering in $AA'BB'X_6$ perovskites should be found when the B' cation is a d^0 transition metal ion in a high oxidation state.

Acknowledgments

The authors acknowledge funding from the National Science Foundation through the Center for the Design of Materials (CHE-043567).

References

[1] C.J. Howard, Acta Crystallogr. A: Found. Crystallogr. 61 (2005) 93–111.
[2] C.J. Howard, B.J. Kennedy, P.M. Woodward, Acta Crystallogr. B: Struct. Sci. 59 (2003) 463–471.
[3] C.J. Howard, H.T. Stokes, Acta Crystallogr. B: Struct. Sci. 60 (2004) 674–684.
[4] P.K. Davies, Curr. Opin. Solid State Mater. Sci. 4 (1999) 467–471.
[5] C. Chaillout, M.A. Alario-Franco, J.J. Capponi, J. Chenavas, J.L. Hodeau, M. Marezio, Phys. Rev. B: Conden. Matter Mater. Phys. 36 (1987) 7118–7120.
[6] C. Chaillout, M.A. Alario-Franco, J.J. Capponi, J. Chenavas, P. Strobel, M. Marezio, Solid State Commun. 65 (1988) 283–286.
[7] P. Karen, P.M. Woodward, J. Linden, T. Vogt, A. Studer, P. Fischer, Phys. Rev. B: Conden. Matter Mater. Phys. 64 (2001) 214405/1–214405/14.
[8] P.M. Woodward, P. Karen, Inorg. Chem. 42 (2003) 1121–1129.
[9] P.M. Woodward, E. Suard, P. Karen, J. Am. Chem. Soc. 125 (2003) 8889–8899.
[10] P. Karen, A. Kjekshus, Q. Huang, V.L. Karen, J.W. Lynn, N. Rosov, I.N. Sora, A. Santoro, J. Solid State Chem. 174 (2003) 87–95.
[11] V. Caignaert, F. Millange, B. Domenges, B. Raveau, E. Suard, Chem. Mater. 11 (1999) 930–938.
[12] F. Millange, V. Caignaert, B. Domenges, B. Raveau, E. Suard, Chem. Mater. 10 (1998) 1974–1983.
[13] A.R. Chakhmouradian, R.H. Mitchell, P.C. Burns, J. Alloys Comp. 307 (2000) 149–156.
[14] B.J. Kennedy, C.J. Howard, Y. Kubota, K. Kato, J. Solid State Chem. 177 (2004) 4552–4556.
[15] A.S. Sefat, G. Amow, M.-Y. Wu, G.A. Botton, J.E. Greedan, J. Solid State Chem. 178 (2005) 1008–1016.
[16] A.G. Belous, J. Eur. Ceram. Soc. 21 (2001) 1797–1800.
[17] A. Rivera, C. Leon, J. Santamaria, A. Varez, M.A. Paris, J. Sanz, J. Non-Cryst. Solids 307–310 (2002) 992–998.
[18] Y. Harada, T. Ishigaki, H. Kawai, J. Kuwano, Solid State Ionics 108 (1998) 407–413.
[19] S. Garcia-Martin, M.A. Alario-Franco, H. Ehrenberg, J. Rodriguez-Carvajal, U. Amador, J. Am. Chem. Soc. 126 (2004) 3587–3596.
[20] C.J. Howard, Z. Zhang, J. Phys.: Conden. Matter 15 (2003) 4543–4553.
[21] C.J. Howard, Z. Zhang, Acta Crystallogr. B 60 (2004) 249–251.
[22] J.H. Park, P.M. Woodward, J.B. Parise, Chem. Mater. 10 (1998) 3092–3100.
[23] L. Dupont, L. Chai, P.K. Davies, Mater. Res. Soc. Symp. Proc. 547 (1999) 93–98.
[24] T. Sekiya, T. Yamamoto, Y. Torii, Bull. Chem. Soc. Japan 57 (1984) 1859–1862.
[25] D.D. Khalyavin, A.M.R. Senos, P.Q. Mantas, J. Phys.: Conden. Matter 17 (2005) 2585–2595.
[26] R.A. Young (Ed.), The Rietveld Method. [In: International Union of Crystallography, Monographs on Crystallography, 1993, p. 5], 1993.
[27] R.W. Cheary, A. Coelho, J. Appl. Crystallogr. 25 (1992) 109–121.
[28] H.T. Stokes, D.M. Hatch, ISOTROPY, 2002.
[29] J. Darriet, S.G. Mayorga, A. Tressaud, Eur. J. Solid State Inorg. Chem. 27 (1990) 783–790.

[30] S.C. Miller, W.F. Love, Tables of Irreducible Representations of Space Groups and Co-representations of Magnetic Space Groups, Pruett, Boulder, 1967.
[31] C.J. Howard, H.T. Stokes, Acta Crystallogr. B 54 (1998) 782–789.
[32] M.A. Arillo, J. Gomez, M.L. Lopez, C. Pico, M.L. Veiga, Solid State Ionics 95 (1997) 241–248.
[33] L. Pauling, J. Am. Chem. Soc. 51 (1929) 1010–1026.
[34] I.D. Brown, Comput. Model. Inorg. Crystallogr. (1997) 23–53.
[35] I.D. Brown, J. Chem. Educ. 77 (2000) 1070–1075.
[36] I.D. Brown, The Chemical Bond in Inorganic Chemistry: The Bond Valence Model, Oxford University Press, Oxford, New York, 2002.
[37] I.D. Brown, D. Altermatt, Acta Crystallogr. B: Struct. Sci. 41 (1985) 244–247.
[38] B.O. Loopstra, P. Boldrini, Acta Crystallogr. 21 (1966) 158–162.
[39] T. Vogt, P.M. Woodward, B.A. Hunter, J. Solid State Chem. 144 (1999) 209–215.
[40] P.M. Woodward, A.W. Sleight, T. Vogt, J. Phys. Chem. Solids 56 (1995) 1305–1315.
[41] J.K. Burdett, Inorg. Chem. 14 (1975) 375–382.
[42] R.G. Pearson, Theochem 12 (1983) 25–34.
[43] A.K. Azad, S.G. Eriksson, A. Mellergard, S.A. Ivanov, J. Eriksen, H. Rundlof, Mater. Res. Bull. 37 (2002) 1797–1813.
[44] Z. Fu, W. Li, Sci. China A: Math. Phys. Astron. 39 (1996) 981–990.
[45] M. Gateshki, J.M. Igartua, J. Phys.: Conden. Matter 15 (2003) 6749–6757.
[46] M. Gateshki, J.M. Igartua, J. Phys.: Conden. Matter 16 (2004) 6639–6649.
[47] D. Iwanaga, Y. Inaguma, M. Itoh, Mater. Res. Bull. 35 (2000) 449–457.
[48] C.P. Khattak, D.E. Cox, F.F.Y. Wang, J. Solid State Chem. 17 (1976) 323–325.
[49] A. Munoz, J.A. Alonso, M.T. Casais, M.J. Martinez-Lope, M.T. Fernandez-Diaz, J. Phys.: Conden. Matter 14 (2002) 8817–8830.
[50] A.M. Glazer, Acta Crystallogr. B: Struct. Sci. B 41 (1972) 244–247.
[51] T. Balic Zunic, I. Vickovic, J. Appl. Crystallogr. 29 (1996) 305–306.